Optical tweezing using tunable optical lattices along a few-mode silicon waveguide

Christophe Pin, J.-B. Jager, M. Tardif, E. Picard, E. Hadji, F. de Fornel, B. Cluzel

Lab on a Chip

ARTICLE

Optical tweezing using tunable optical lattices along a few-mode silicon waveguide

Received 00th January 20xx,
Accepted 00th January 20xx

DOI: 10.1039/x0xx00000x

www.rsc.org/

C. Pin,[a,b,‡] J.-B. Jager,[b] M. Tardif,[b] E. Picard,[b] E. Hadji,[b] F. de Fornel[a] and B. Cluzel*[a]

Fourteen years ago, optical lattices and holographic tweezers were considered as a revolution, allowing for trapping and manipulating multiple particles at the same time using laser light. Since then, near-field optical forces have aroused tremendous interest as they enable efficient trapping of a wide range of objects, from living cells to atoms, in integrated devices. Yet, handling at will multiple objects using a guided light beam remains a challenging task for current on-chip optical trapping techniques. We demonstrate here on-chip optical trapping of dielectric microbeads and bacteria using one-dimensional optical lattices created by near-field mode beating along a few-mode silicon nanophotonic waveguide. This approach allows not only for trapping a large number of particles in periodic trap arrays with various geometries, but also for manipulating them via diverse transport and repositioning techniques. Near-field mode-beating optical lattices may be readily implemented in lab-on-a-chip devices, addressing numerous scientific fields ranging from bio-analysis to nanoparticle processing.

Introduction

The mechanical action of light on matter was experimentally demonstrated by A. Ashkin in 1970 (1). His seminal work provided a perfect illustration of how optical forces can help to overcome the Brownian diffusion of particles in solution, by either accelerating or trapping them. These two aspects of optical forces have since inspired numerous and fertile research studies dedicated to optical trapping and manipulation (2-4). Recently, near-field optical forces have aroused tremendous interest as they offer unique advantages such as enhanced gradient forces, sub-diffraction limit resolution, and on-chip applications. Efficient trapping, handling, guiding, and sorting of particles, ranging from atoms to living cells, have been already demonstrated in miscellaneous experiments using plasmonic and photonic structures (4-8).

Nevertheless, development of near-field optical tweezers still faces some critical challenges. One of them consists in being able to precisely manipulate a large ensemble of trapped particles, by simultaneously controlling both their collective and singular motions using guided light. While far-field optical tweezers can managed this task using optical lattices, time-shared laser traps, or holographic optical traps (2-3), efficient equivalent techniques are still desired for on-chip optical trapping. Two main approaches have been investigated heretofore (8). The first one consists in using the light propagating in a waveguide to trap and propel particles as on a conveyor belt (4,5,9-16). However, this strategy usually fails whenever trapped particles' propulsion has to be stopped, requiring more complex and restrictive implementation based on irregular waveguide geometries (17), microfluidic channel walls (18), or counter-propagating modes (8,19-24). On the other hand, the second approach is based on micro- or nanoscale much localized resonant phenomena, relying either on resonant modes in photonic crystals and cavities (4,5,7,8,25-31) or on localized surface plasmon resonances (4,6,7,32-38). By concentrating the electromagnetic field intensity in sub-wavelength volumes, this approach allows efficient but rather static optical trapping. Especially, particle manipulation using plasmonic nanotweezers integrated on optical waveguides has not been demonstrated yet (37,38).

Therefore, new versatile techniques are needed for being able to directly trap, order, and transport at will large numbers of single objects in a optofluidic lab-on-a-chip. We demonstrate here a flexible, all-optical approach for large scale on-chip multi-particle trapping and manipulation. We first evidence that when two modes with different propagation constants co-propagate in a few-mode silicon waveguide, the resulting near-field mode beating creates a spatial modulation of optical forces, making it possible to generate one-dimensional optical lattices with various mode- and wavelength-dependent spatial configurations. Although such a similar approach was already envisaged in few theoretical works dealing with atom trapping (39-44) and demonstrated with the help of a counter-propagating beam in a hollow-core

[a] Groupe Optique de Champ Proche, Laboratoire Interdisciplinaire Carnot de Bourgogne UMR CNRS 6303, Université de Bourgogne Franche-Comté, 21078 Dijon, France. Tel: +33 3 80 39 60 10; E-mail: benoit.cluzel@u-bourgogne.fr
[b] Univ. Grenoble Alpes, CEA, INAC, PHELIQS, SINAPS, F-38000 Grenoble, France.
† Electronic Supplementary Information (ESI) available: Supplementary Figures and 2 Supplementary Movies. See DOI: 10.1039/x0xx00000x
‡ Present address: Research Institute for Electronic Science, Hokkaido University, Sapporo, Hokkaido, 001-0020, Japan.
ORCID iD: 0000-0002-5088-5711

photonic crystal fibre (45), it is here experimentally implemented for tweezing microscale and sub-microscale objects such as dielectric particles and bacteria on a photonic chip. Some on-chip manipulation methods based on near-field mode-beating lattices are also illustrated. First, on-demand switching between different trapping configurations is achieved by dynamically controlling the excitation of the different guided modes. Then, we show that tuning the excitation wavelength makes it possible to modify at will the lattice period over hundreds of nanometres. Besides, we demonstrate that a pulling force can be applied to all the trapped particles by gradually decreasing the laser wavelength, the near-field optical lattice acting thus as an on-chip tractor beam. Our experimental results highlight the high degree of modal and spectral tunability of near-field mode-beating optical lattices, paving the way for further development and applications.

Experimental

Optical force modulation via near-field mode beating

Silicon-on-insulator (SOI) nanophotonic waveguides allow at the same time for high lateral confinement and low-loss propagation of light at telecommunication wavelengths (46). Interestingly, light confinement results in strong evanescent fields, and thus in enhanced near-field optical forces (4,5,7,8). Nanophotonic waveguides also enable modal multiplexing of guided light at the nanoscale by allowing light propagation through a set of orthogonal guided modes with different propagation constants (46). For instance, rectangular cross-section nanophotonic waveguides are well-known to support both quasi-transverse-electric (TE-like) and quasi-transverse-magnetic (TM-like) modes, the number of which depends on the waveguide's width and height (46). Although orthogonality prevents copropagating modes from interfering with each other, the local phase difference between their evanescent tails causes various near-field light-matter interactions (43,47-50), including optical forces (10), to be subject to near-field mode-beating phenomena. When two co-propagating guided modes are excited, a periodic spatial modulation of the optical force field appears along the waveguide, with a characteristic beat period (43,47,49,50):

$$p_{ij} = \frac{2\pi}{\left|\beta^{(i)} - \beta^{(j)}\right|} = \frac{\lambda_0}{\left|{n_{eff}}^{(i)} - {n_{eff}}^{(j)}\right|}$$

where λ_0 refers to the free-space wavelength and $\beta^{(i)}$, $\beta^{(j)}$ (respectively ${n_{eff}}^{(i)}$, ${n_{eff}}^{(j)}$) to the propagation constant (respectively to the effective refractive index) of the two guided modes.

In this work, we consider few-mode SOI waveguides with 510 x 248 nm² rectangular cross-sections, fabricated by standard microelectronics fabrication process. The waveguide's width was chosen in order to maximize the difference in effective index between the three guided modes, particularly between the TE1 mode and each fundamental mode, in order to minimize their beating lengths (see Supplementary Information). As shown in Fig. 1(a), three guided modes are supported by such waveguides in the 1530-1560 nm wavelength range: the TE0 and TM0 fundamental modes and the first order TE1 longitudinal mode. Three pair combinations can be obtained from these guided modes, leading to three distinct near-field mode beating distributions. For each case, horizontal and vertical cross-sections of the effective near-field intensity (squared modulus of the vectorial sum of all excited modes' evanescent fields) are plotted in Fig. 1(c). Although near-field beating of the two fundamental modes only results in a slight lateral undulation of the top-surface effective near-field intensity (see Supplementary Information), clear periodic modulation of the effective near-field intensity appears along the waveguide's side walls (respectively top surface) as the TE1 mode is beating with the

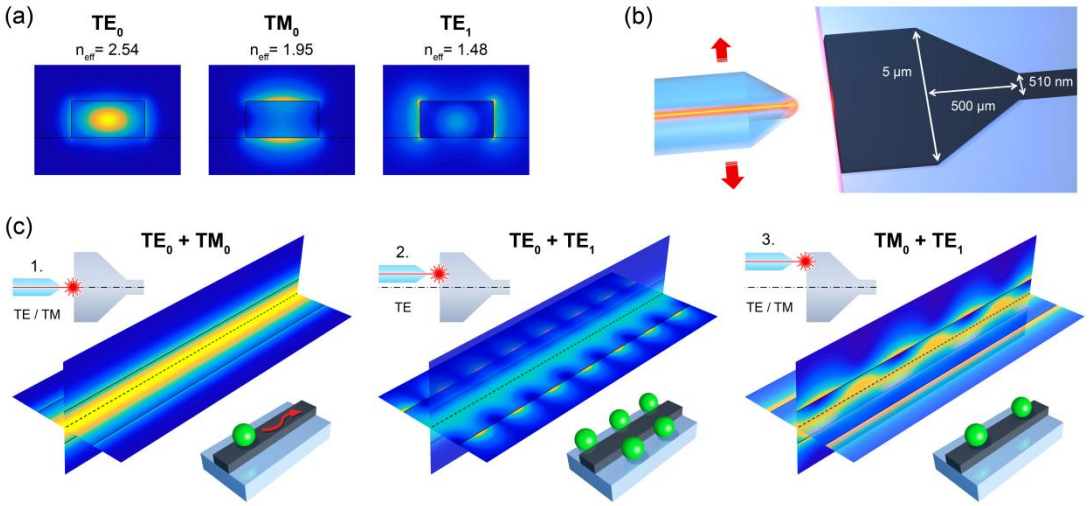

Fig. 1 Near-field mode beating in a few-mode silicon waveguide. (a) Intensity profile and effective indices of the three guided modes supported by a 510 x 248 nm2 silicon waveguide at telecom wavelengths (1530 nm), calculated by Finite-Element Method. (b) Schematic representation of the light coupling set-up used in this work. (c) Horizontal and vertical cross-sections of the effective intensity distribution resulting from the copropagation of, respectively, the TE0-TM0, the TE0-TE1, and the TM0-TE1 modes along a 10-µm-long portion of waveguide. For each case, light coupling conditions at the entrance of the waveguide are indicated: 1. Fibre centred and excitation of both polarization components; 2. Fibre slightly off-axis and excitation of the horizontal polarization component only; 3. fibre off-axis and excitation of both polarization components. The behaviour of particles trapped at the surface of the waveguide is also schematically depicted.

TE0 mode (respectively TM0 mode). In the low-perturbation approximation, the effective near-field intensity can be straightforwardly considered as proportional to the trapping potential experienced by Rayleigh particles. As shown in previous work, this hypothesis still holds true for microbeads about one wavelength in diameter (30). Such patterning of the trapping potential gives birth to periodic arrays of potential wells that can be advantageously used for the practical realization of on-chip optical lattices.

Experimental details

Photonic waveguides were fabricated by standard electron-beam lithography and reactive ion etching process, using SOI wafers with a 248-nm-thick silicon top-layer and 2-µm-thick buried oxide layer. Photonic chips were then cleaved using a manual indent-and- cleaving apparatus. After fabricating a PDMS film on a clean silicon wafer, a thin PDMS spacer was cut, peeled off, and placed on the top surface of a photonic chip. The microfluidic chamber is then filled by depositing a drop of colloidal solution containing green fluorescent polystyrene microbeads (Thermo Scientific Fluoro-max Dyed Green Aqueous Fluorescent Particles) in water or Escherichia Coli (E. Coli) bacteria in API Suspension medium (bioMérieux). Initial colloidal suspensions of polystyrene microbeads and bacteria were diluted in pure water prior to all trapping experiments. A piece of glass coverslip was eventually placed above the chamber in order to seal it while still allowing for the observation of particles' motion using a home-made microscope (28, 30).

In order to perform all near-field optical trapping experiments, light from a fibered tunable laser source (TUNICS, Yenista Optics) emitting at telecommunication wavelengths was amplified by an erbium-doped fibre amplifier with an output power up to 224 mW in the C-band (wavelengths ranging from 1529 to 1565 nm). A polarization-maintaining optical fibre with a lensed tip was used to couple the laser light into photonic waveguides via the cleaved input facet of the photonic chip, as shown in Fig. 1(b). Considering the different optical losses and the intensity of the transmitted signal measured at the output of the waveguide, the coupling efficiency between the fibre and the silicon waveguide was estimated of the order of 0.1. Excitation of the selected guided modes was achieved by controlling both the polarization of the incoming laser light and the lensed fibre tip's position relatively to the cleaved facet of a 5-µm-large waveguide section by using a 3-axis piezo-stage (51). Following the 5-µm-large waveguide section, a 500-µm-long linearly tapered waveguide section was then used to couple the light to a few-mode nanophotonic waveguide, as described in Fig. 1(b). The transmitted light was collected from the cleaved output facet of the photonic chip using a 15X Cassegrain microscope objective and an InGaAs photodiode in order to monitor the coupling and transmission efficiency of waveguides. A home-built fluorescence microscope, composed of a long-working distance 50X microscope objective (M Plan APO HR, Mitutoyo), a 12X Navitar UltraZoom-motorized lens tube, and a monochrome CCD camera (Prosilica GC 1290, AVT), was used to observe and record the motion of trapped objects (28, 30).

Optical trapping analysis

Video of optical trapping experiments were recorded with a frame rate of 24 fps. Particle tracking and optical trapping potential mapping (see Supplementary Information) were performed according to previously published methods (30). Kymographs were obtained as follow: For each recorded image, few pixel lines showing the array of trapped particles (from 10 to 25 lines, depending on the particles' size, as well as the magnification and illumination conditions) were averaged in order to form a single line of pixels. All averaged pixel lines were then appended one below each other, following the chronological order of the initial image sequence (see Supplementary Movie S1).

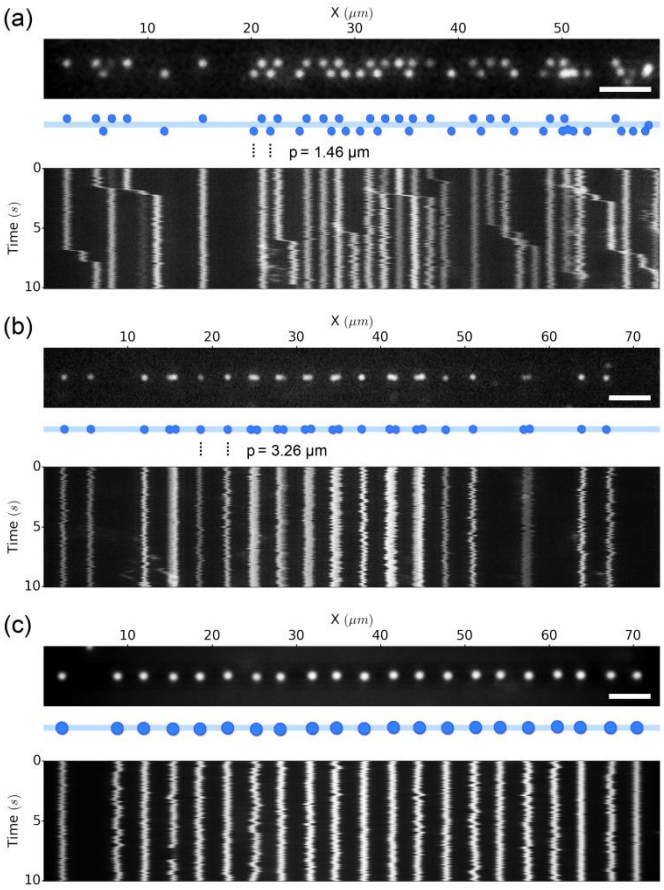

Fig. 2 Optical trapping of dielectric particles using near-field optical lattices. Fluorescence images and corresponding kymographs (upper row) of (a) 500 nm fluorescent polystyrene beads trapped in a TE0-TE1 lattice, (b) 500 nm fluorescent polystyrene beads trapped in a TM0-TE1 lattice, and (c) 1 µm fluorescent polystyrene beads trapped in a TM0-TE1 lattice (wavelength: 1530 nm, source power: 224 mW, scale bars: 5 µm). Trapped beads are schematically represented in blue on each diagram.

Results

Near-field mode beating optical lattices

By testing the various light coupling conditions described in Fig. 1(c), it was possible to observe three different trapping regimes. The first one (not shown here), presumably resulting from the predominant propagation of both TE0 and TM0 modes, is characterized by the trapped particles being continuously propelled along the waveguide under the action of the scattering force, as in single excited mode's cases (4). However, as shown in Fig. 2, the two other trapping regimes correspond to well-defined stable periodic arrangements of trapped particles, either positioned in staggered rows on both side of the waveguide or aligned in a single row above the waveguide's top surface. Not only are these patterns consistent with numerical predictions presented in Fig. 1, but experimental values of lattice periods reported in Fig. 2(a) and 2(b) are also in good agreement with theoretical values deduced from equation (1) (1.46 µm and 3.27 µm, respectively). Hence, it can be inferred that the former lattice results from the predominant propagation of TE0 and TE1 modes, while the latter arises from the predominant propagation of TM0 and TE0 modes. Although both 500 nm (Fig. 2(b)) and 1µm (Fig. 2(c)) beads were successfully trapped in the TM0-TE1 lattice configuration, only 500 nm beads (Fig. 2(a)) were observed to be trapped in the TE0-TE1 lattice configuration. A possible reason for it lies in the geometrically restricted access to the near-field of the waveguide's side walls due to the substrate's surface.

The stability of the optical traps can be observed on kymographs plotted in Fig. 2, and displaying the time evolution of the trapped particles' location along the waveguide (see Supplementary Movie S1). The TM0-TE1 lattice was found to be particularly efficient, allowing for stable trapping of particles over several minutes (see Supplementary Information). The relatively large period of the TM0-TE1 lattice, compared to the waveguide's width, results in optical traps with an elongated shape, as evidenced by Fig. 3(b). This explains why, in Fig. 2(b), several 500 nm beads are sometimes trapped together at the same time in the same potential well. As for the trapping efficiency, values of trap's stiffness as high as 9.6 ± 2.6 fN.nm-1 (lateral stiffness) and 0.85 ± 0.25 fN.nm-1 (longitudinal stiffness) were measured in the case of 500 nm beads, while 1 µm beads were found to experience trap stiffnesses reaching 3.6 ± 1.3 fN.nm-1 (lateral stiffness) and 0.2 ± 0.1 fN.nm-1 (longitudinal stiffness).

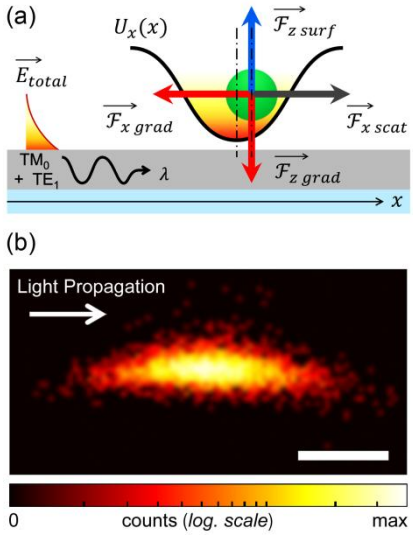

Fig. 4 Force equilibrium and trapping potential. (a) Schematic representation of the forces acting on a particle trapped in a TM0-TE1 lattice. (b) Experimental map of the trapping potential experienced by a 1 µm bead in a TM0-TE1 lattice (scale bar: 250 nm).

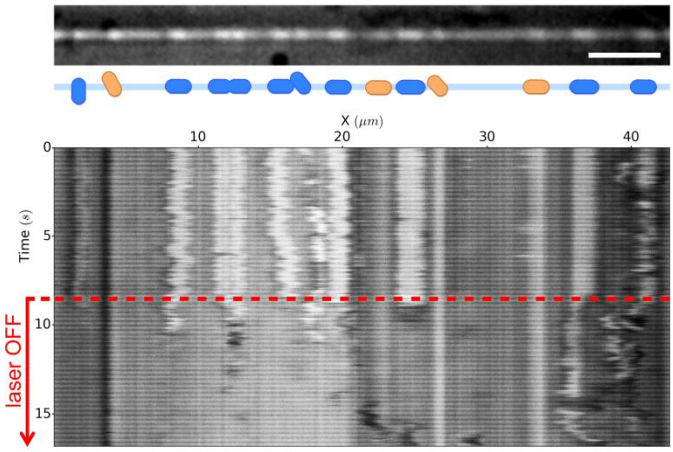

Fig. 3 Optical trapping of bacteria using near-field optical lattices. Optical trapping of bacteria using near-field optical lattices. Bright-field image and kymograph of bacteria (E. Coli) trapped by exciting both TM0 and TE1 modes (wavelength: 1550 nm, source power: 100 mW, scale bar: 5 µm). Bacteria schematically depicted in orange on the diagram were adsorbed on the waveguide's surface, while others (in blue) were trapped by optical forces. The laser source was switched off after 8 s in order to release the trapped bacteria.

To emphasize the miscellaneous potential applications of near-field mode beating lattices, successful trapping of bacteria (E. Coli) was demonstrated using a TM0-TE1 lattice configuration, as can be seen in Fig. 4. Despite the lower image quality compared to previous experiments with fluorescent microbeads, stable trapping and release of multiple bacterium cells is evidenced on the kymograph shown in Fig. 4 (see Supplementary Movie S1). Although optical forces acting on bacterium cells are expected to differ from forces acting on spherical microbeads, these results proves that near-field mode beating remains a suitable approach for on-chip optical trapping of biological objects as well as particles with non-spherical shapes.

Interestingly, as can be seen in Fig. 2(a), particles are sometimes observed to jump from one trap to another located downstream. To understand this phenomenon, one should keep in mind that trapped particles are still experiencing propulsive scattering force due to light propagation. In Fig. 3(a), we schematically review the forces acting on a particle trapped in a TM0-TE1 lattice. The potential well along the vertical axis results from the equilibrium between the attractive optical gradient force and repulsive electrostatic surface interactions (16). Light propagation also imparts a forward scattering force that tends to propel the particle along

the waveguide, while a lateral gradient force maintains the particle centered above the waveguide's top surface (9). However, near-field mode beating gives rise to an additional modulation of the gradient force, whose intensity and direction periodically vary along the waveguide. As evidenced by our experimental results, the intensity of this gradient force can be high enough to counterbalance the propulsive scattering force. As in the case of standard single-beam optical tweezers, an equilibrium state can thus be reached, allowing for stable three-dimensional optical trapping. The same situation occurs here periodically along the waveguide, leading to the creation of a large number of optical traps.

The stability of the equilibrium described in Fig. 3(a) can nonetheless be perturbed by the arrival of an additional particle. As illustrated by Fig. 5(a) in the case of 1 µm beads trapped in a TM0-TE1 lattice, such a phenomenon induces a cascaded displacement of all particles occupying downstream traps within the lattice (see Supplementary Movie S2). As an incoming particle reaches the first already occupied upstream trap, this newly trapped particle competes with the one previously trapped, driving the system unstable. Because of the asymmetry introduced by the scattering force, the initially trapped particle is ejected from the trap, and propelled downstream. When reaching the next trap, it leads in turn to the ejection of the previously trapped particle, and the same mechanism repeats itself along the waveguide. Although this cascaded process spontaneously occurred in our experiment, one can already envision its implementation in a more advanced microfluidic environment for on-demand single-particle delivery or logic manipulation of microparticles, as inspired by recent progress in droplet and bubble microfluidics (52).

On-chip optical manipulation techniques

While some additional microfluidic technique could be advantageously used to deterministically control the cascaded

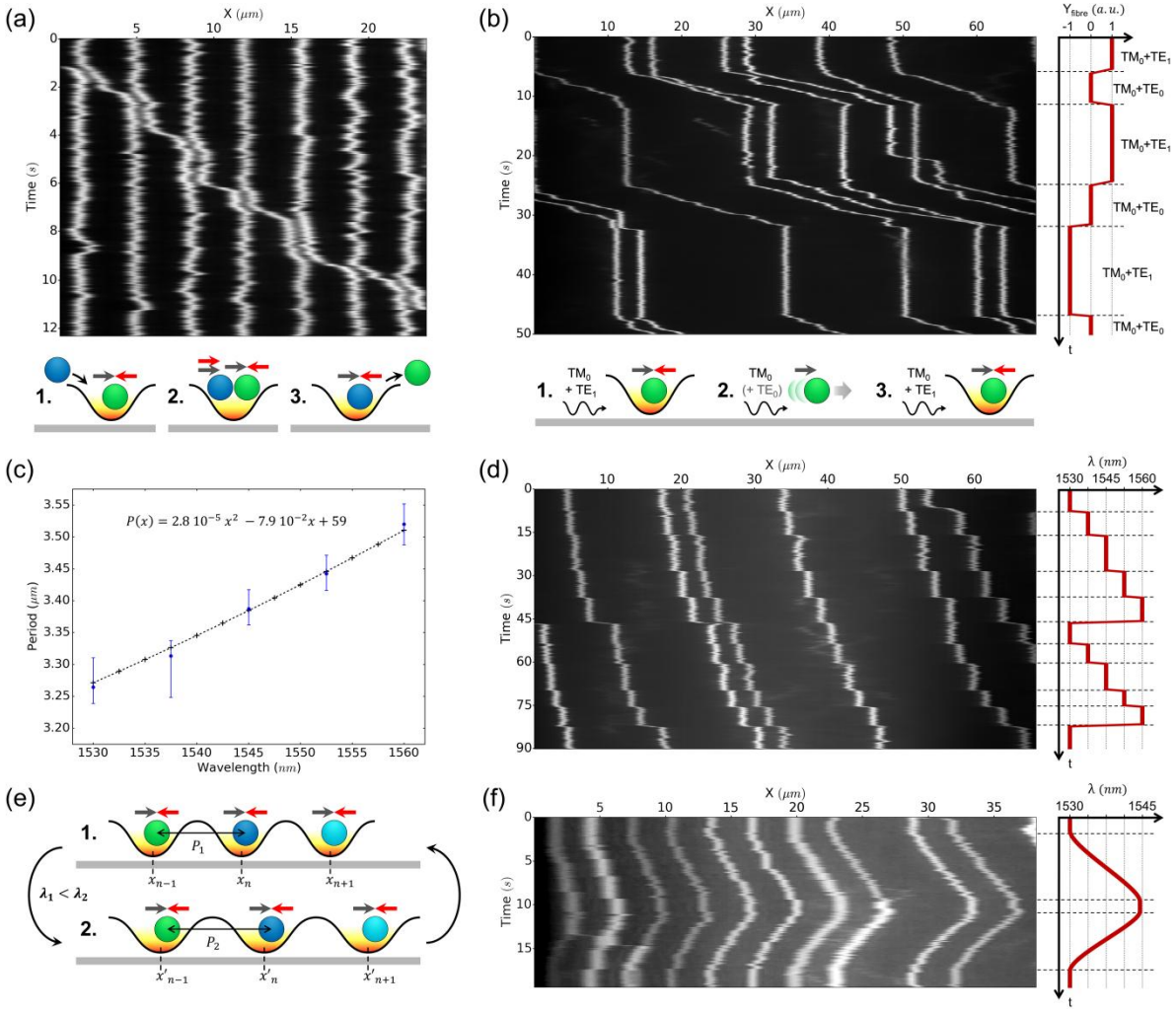

Fig. 5 On-chip optical manipulation of trapped particles. (a) Kymograph and diagram illustrating a cascaded process leading to the discrete displacement of all the 1 µm beads trapped in a TM_0-TE_1 lattice. (b) Kymograph and diagram illustrating the successive propulsion and static trapping of 1 µm beads by alternating the excitation of TM_0-TE_0 and TM_0-TE_1 modes. (c) Period of the TM_0-TE_1 lattice as a function of the wavelength. The black dashed curve is a parabolic fit of calculated values (black crosses). Experimental values (blue points) were obtained from the kymograph shown in (d). (d) Kymograph evidencing the spectral tunability of a TM_0-TE_1 lattice. The position of trapped 1 µm beads is successively moved downstream along the waveguide by applying discrete wavelength changes. (e) Diagram and (f) kymograph describing the continuous two-way transport and repositioning of 500 nm beads trapped in a TM_0-TE_1 lattice by gently varying the wavelength.

displacement process depicted in Fig. 5(a), we rather explore in this work the unique optical properties of near-field mode beating lattices and their applications to all-optical on-chip manipulation of trapped particles. A first possible way to handle the trapped particles lies in the dynamic control of the guided mode excitation. For instance, repeatedly switching from TM0-TE1 to TE0-TM0 excitation (or to any single mode excitation) makes it possible to alternate between static trapping and propulsion. In practice, modal selection was experimentally achieved by sequentially modifying the lensed fiber tip's position relatively to the waveguide's input facet. As shown in Fig. 5(b), the different light coupling conditions lead to the successive excitation of either TM0-TE1 or TE0-TM0 modes, allowing us to stop (fiber off-centered) and start again (fiber centered) on demand the particle transportation along the waveguide (see Supplementary Movie S2). Fig. 5(b) also illustrates the phase control of the trap position, a technique first demonstrated by Soltani, M. et al. (23). Here, a π-shift in the TE1 mode excitation was observed when moving the fiber tip from one side to the other side of the waveguide's input facet, leading to a half-period shift of the lattice.

Spectral tunability is another interesting feature of near-field mode beating lattices. Owing to the mode-dependent waveguide dispersion, modifying the laser wavelength affects the effective index difference between excited modes, hence the lattice period. As shown in Fig. 5(c), this property was experimentally and numerically verified in the case of the TM0-TE1 lattice. From experimental data presented in Fig. 5(d) (see Supplementary Movie S2), it was found that any wavelength shift results in a variation of the lattice period about height time larger, in good agreement with numerical results. Thus, the lattice period can be optically tuned over a few hundred nanometers with a few picometers' theoretical resolution by using a tunable laser source emitting at telecommunication wavelengths with a 1 pm tuning step. As illustrated in Fig. 5(e), this spectral tunability provides a unique opportunity to manage both positioning and transport of all trapped particles along the waveguide. In the first place, each trap can be displaced with amplitude that depends on the trap's position in the lattice. Considering in first approximation a fixed phase difference between the excited modes at the nanophotonic waveguide's entrance, the m-th trap's displacement is m times larger than a single period's variation. Thus, depending on required specifications, one should consider using either traps located near the waveguide's entrance, which can be positioned with sub-nanometer precision, or traps located farther downstream, which can be displaced over tenths of micrometers. The only physical restriction for the displacements' range lies in propagation losses, especially as regards to the near-cutoff TE1 mode.

Hydrodynamic drag also plays a key role in the particle manipulation process. Indeed, for particles to accurately follow the traps' displacements, care should be taken to handle them gently in order to preserve the trapping equilibrium condition. As demonstrated in Fig. 5(f), this can be achieved by continuous and slow enough wavelength variations, enabling the practical realization of an on-chip tractor beam (see Supplementary Movie S2). However, the drag force can be advantageously used to reposition the particles in the trap lattice (23). In Fig. 5(d), when the initial wavelength is rapidly restored, every particle moves downstream until another nearby trap is reached. This behavior can be well explained by the fact that, as traps are suddenly moved backward along the waveguide, the sum of hydrodynamic drag and optical scattering forces surpasses the moving traps' restoring force. As evidenced here, this effect can be used to manage long range transportation of trapped particles. Besides, it was observed that fast wavelength scanning combined with hydrodynamic damping can even be used to influence the velocity of continuously transported particles (see Supplementary Information).

Conclusions

We have shown in this work how on-chip optical lattices can be obtained from near-field beating of orthogonal guided modes in a few-mode nanophotonic waveguide. The local phase difference between each mode's near-field results in periodic modulation of optical forces in the vicinity of the waveguide. By exciting selected pairs of copropagating modes, we have demonstrated that near-field optical lattices with different geometries and periods can be created. Stable trapping of large ensemble of polystyrene microbeads and bacteria has been achieved with average trap stiffnesses in the $fN.nm^{-1}$ range, which is comparable to values found in the literature dealing with photonic and plasmonic trapping (23,29,30,33). Although optical lattices along a waveguide requires a laser power higher than single optical traps in the near-field of resonant photonic or plasmonic nanostructures, this increase should be related to the number of traps created. Compared with previous work on photonic crystal cavities (30), lattices with more than 50 optical traps have been generated by increasing the laser power only by a factor 10 to 20. Besides, significant improvement in the trapping efficiency may be achieved by using optimized photonic mode-multiplexing solutions dedicated to the controlled excitation of guided modes. New trapping configurations can be also envisaged in order to decrease the laser power required for stable optical trapping. For instance, pairs of counterpropagating orthogonal modes would certainly help to reduce, or even cancel the scattering force effects. The approach proposed here may be also advantageously combined with previously reported nanophotonic standing-wave array trap (23) in order to increase the optical traps' longitudinal stiffness.

The trapping approach proposed here enables on-chip handling of large ensembles of trapped particles by various manipulation techniques. By modifying the mode excitation conditions, on-demand switching between stable trapping and propulsion of particles has been achieved. We have also evidenced how the lattice period can be tuned by controlling the wavelength. Both pushing and pulling forces can be applied to the trapped particles, allowing for all-optical transport and repositioning. Both of these modal and spectral

techniques come in addition to already reported phase-difference control (23) and could be advantageously combined with other mechanisms as suggested for cascaded displacement of particles. By making use of such trapping based optical manipulation techniques, simple nanophotonic waveguides can be turned into versatile on-chip conveyor belts, capable of handling particles along nanoscale assembly lines. Implemented in labs- or factories-on-chips, this technology could bridge the gap between nanoscale operations ruled by thermal fluctuations and deterministically planned processes at the micro- or even macroscale.

Eventually, we expect this work to pave the way for further developments in a wide range of scientific fields, with applications ranging from reconfigurable medical lab-on-a-chip applications (8,11,23) and even cold-atom physics (39,41,43,44). It should be also highlighted that, although our work is based on silicon nanophotonic waveguides with rectangular cross-section, design principles described here could be advantageously adapted to other materials and waveguide geometries. For instance, creating near-field optical lattices along silicon nitride waveguides would be of particular interest for biological and visible-light-based applications (8,24).

Conflicts of interest

There are no conflicts to declare.

Acknowledgements

C.P. thanks O. Demichel and A. Coillet for their useful advice. J.B.J. thanks N. Pauc and J.L. Thomassin for helpful technical discussions on nanofabrication. This work was performed in cooperation with the Labex ACTION program (contract ANR-11-LABX-0001-01), and with the support of the “Plateforme Technologique Amont” of Grenoble, funded through the CNRS Renatech network.

References

1 A. Ashkin, *Phys. Rev. Lett.*, 1970, **24**, 156-159.
2 D.G. Grier, *Nature*, 2003, **424**, 810-816.
3 K. Dholakia and T. Čižmár, *Nat. Photon.*, 2011, **5**, 335-342.
4 M. Daly, M. Sergides and S.N. Chormaic, *Laser Photon. Rev.*, 2015, **9**, 309-329.
5 D. Erickson, X. Serey, Y.F. Chen and S. Mandal, *Lab Chip,* 2011, **11**, 995-1009.
6 M.L. Juan, M. Righini and R. Quidant, *Nat. Photon.* 2011, **5**, 349-356.
7 D. Conteduca, F. Dell’Olio, T.F. Krauss and C., *Appl. Spectrosc.*, 2017, **71**, 367-390.
8 J.E. Baker, R.P. Badman and M.D. Wang, *WIREs Nanomed. Nanobiotechnol.*, 2017, e1477.
9 S. Kawata and T. Tani, *Opt. Lett*., 1996, **21**, 1768-1770.
10 T. Tanaka and S. Yamamoto, *Jpn. J. Appl. Phys.*, 2002, **41**, L260.
11 S. Gaugiran, S. Gétin, J.M. Fedeli, G. Colas, A. Fuchs, F. Chatelain and J. Dérouard, *Opt. Express*, 2005, **13**, 6956-6963.
12 A.H. Yang, S.D. Moore, B.S. Schmidt, M. Klug, M. Lipson and D. Erickson, *Nature*, 2009, **457**, 71-75.
13 L.C. Hsu, T.-C. Chen, Y.-T. Yang, C.-Y. Huang, D.-W. Shen, Y.-T. Chena and M.-C.M. Lee, *Lab Chip*, 2013, **13**, 1151-1155.
14 M.G. Scullion, Y. Arita, T.F. Krauss and K. Dholakia, *Optica*, 2015, **2**, 816-821.
15 A. Maimaiti, D. Holzmann, V.G. Truong, H. Ritsch and S.N. Chormaic, *Sci. Rep.*, 2016, **6**, 30131.
16 P. Schein, D. O'Dell and D. Erickson, *ACS Photonics*, 2017, **4**, 106-113.
17 H. Cai and A.W. Poon, *Lab Chip*, 2012, **12**, 3803-3809.
18 K.D. Leake, M.A. Olson, D. Ozcelik, A.R. Hawkins and H. Schmidt, *Opt. Lett.*, 2015, **40**, 5435-5438.
19 K. Grujic and O.G. Hellesø, *Opt. Express*, 2007, **15**, 6470-6477.
20 A. Goban, K.S. Choi, D.J. Alton, D. Ding, C. Lacroûte, M. Pototschnig, T. Thiele, N.P. Stern and H.J. Kimble, *Phys. Rev. Lett.*, 2012, **109**, 033603.
21 P. Schneeweiss, S.T. Dawkins, R. Mitsch, D. Reitz, E. Vetsch and A. Rauschenbeutel, *Appl. Phys. B*, 2013, **110**, 279-283.
22 C.F. Phelan, T. Hennessy and T. Busch, *Opt. Express*, 2013, **21**, 27093-27101.
23 M. Soltani, J. Lin, R.A. Forties, J.T. Inman, S.N. Saraf, R.M. Fulbright, M. Lipson and M.D. Wang, *Nat. Nanotech*., 2014, **9**, 448-452.
24 F. Ye, R.P. Badman, J.T. Inman, M. Soltani, J.L. Killian and M.D. Wang, *Nano Lett*., 2016, **16**, 6661-6667.
25 C. Renaut, J. Dellinger, B. Cluzel, T. Honegger, D. Peyrade, E. Picard, F. de Fornel and E. Hadji, *Appl. Phys. Lett.*, 2012, **100**, 101103.
26 C. Renaut, B. Cluzel, J. Dellinger, L. Lalouat, E. Picard, D. Peyrade, E. Hadji and F. de Fornel, *Sci. Rep.*, 2013, **3**, 2290.
27 N. Descharmes, U.P. Dharanipathy, Z. Diao, M. Tonin and R. Houdré, *Lab Chip*, 2013, **13**, 3268-3274.
28 C. Pin, B. Cluzel, C. Renaut, D. Peyrade, E. Picard, E. Hadji and F. de Fornel, *Appl. Phys. Lett.*, 2014, **105**, 171108.
29 L. Milord, E. Gerelli, C. Jamois, A. Harouri, C. Chevalier, P. Viktorovitch, X. Letartre and T. Benyattou, *Appl. Phys. Lett.*, 2015, **106**, 121110.
30 C. Pin, B. Cluzel, C. Renaut, E. Picard, D. Peyrade, E. Hadji and F. de Fornel, *ACS Photonics*, 2015, **2**, 1410-1415.
31 S.H. Wu, N. Huang, E. Jaquay and M.L. Povinelli, *Nano Lett.*, 2016, **16**, 5261-5266.
32 W. Zhang, L. Huang, C. Santschi and O.J. Martin, *Nano Lett*., 2010, **10**, 1006-1011.
33 Y. Tanaka, S. Kaneda and K. Sasaki, *Nano Lett.*, 2013, **13**, 2146-2150.
34 J. Berthelot, S.S. Aćimović, M.L. Juan, M.P. Kreuzer, J. Renger and R. Quidant. *Nat. Nanotech.*, 2014, **9**, 295-299.
35 Y. Zheng, J. Ryan, P. Hansen, Y.-T. Cheng, T.-J. Lu and L. Hesselink, *Nano Lett.*, 2014, **14**, 2971-2976.
36 P.T. Lin, H.Y. Chu, T.W. Lu and P.T. Lee, *Lab Chip*, 2014, **14**, 4647-4652.
37 G. Wang, Z. Ying, H.-P. Ho, Y. Huang, N. Zou, X. Zhang, *Opt. Lett*., 2016, **41**, 528-531.
38 G. Magno, A. Ecarnot, C. Pin, V. Yam, P. Gogol, R. Mégy, B. Cluzel and B. Dagens, *Opt. Lett.*, 2016, **41**, 3679-3682.
39 K. Christandl, G.P. Lafyatis, S.C. Lee and J.F. Lee, *Phys. Rev. A*, 2004, **70**, 032302.
40 F. Le Kien, V.I. Balykin and K. Hakuta, *Phys. Rev. A*, 2004, **70**, 063403.
41 J. Fu, X. Yin and L. Tong, *J. Phys. B*, 2007, **40**, 4195-4210.
42 G. Sagué, A. Baade and A. Rauschenbeutel, *New J. Phys.*, 2008, **10**, 113008.
43 T.H. Stievater, D.A. Kozak, M.W. Pruessner, R. Mahon, D. Park, W.S. Rabinovich and F.K. Fatemi, *Opt. Mat. Express*, 2016, **6**, 3826-3837.

44 M. Sadgrove, S. Wimberger and S.N. Chormaic, *Sci. Rep.*, 2016, **6**, 28905.
45 O. A. Schmidt, T. G. Euser and P. S. J. Russell, *Opt. Express*, 2013, **21**, 29383-29391.
46 K. Yamada, T. Tsuchizawa, H. Fukuda, C. Koos, J. Pfeifle, J.H. Schmid, P. Cheben, P.J. Bock and A.P. Knights, in *Handbook of silicon photonics*, ed. L. Vivien and L. Pavesi, CRC Press, Taylor & Francis, Boca Raton, Florida, 2013, Chap. 2, 55-96.
47 M.L.M. Balistreri, A. Driessen, J.P. Korterik, L. Kuipers and N.F. Van Hulst, *Opt. Lett.*, 2000, **25**, 637-639.
48 M.L.M. Balistreri, J.P. Korterik, L. Kuipers and N.F. Van Hulst, *Phys. Rev. Lett.*, 2000, **85**, 294-297.
49 K. Gut, *Acta Phys. Pol. A*, 2013, **124**, 425-427.
50 B.D. Jennings, D. McCloskey, J.J. Gough, T. Hoang, N. Abadía, C. Zhong, E. Karademir, A.L. Bradley and J.F. Donegan, *J. Opt.*, 2017, **19**, 015604.
51 K. Grujic, O.G. Hellesø, J.P. Hole and J.S. Wilkinson, *Opt. Express*, 2005, **13**, 1-7.
52 M. Prakash and N. Gershenfeld, *Science*, 2007, **315**, 832-835.

